Benha Journal of Engineering Science and Technology

كلية الهندســـة ببنها
FACULTY OF ENGINEERING- BENHA

Egyptian Knowledge Bank
بنك المعرفة المصري

https://bjest.journals.ekb.eg/

Evaluation of Seismic Separation Distance of the ECP Using Nonlinear Time History Analysis

Mohamed A. Abd El-Aziz [a], Amr R. El-Gamal [a], Ahmed M. Abd El-Salam [a], Hala M. Refaat [a]
[a] *Civil Engineering Department, Benha Faculty of Engineering, Benha University, Egypt.*

Keywords:
Seismic pounding
Separation distance
Nonlinear time history analysis
Ground motion records
Earthquake engineering
Adjacent buildings

A B S T R A C T

Adequate seismic separation distance between adjacent buildings is essential to prevent seismic pounding, which remains one of the most critical sources of damage in densely constructed urban areas. Many codes, including the Egyptian Code for Loads ECP 201, rely on simplified displacement-based formulas that may not fully capture the complex dynamic interaction between neighboring structures. This study evaluates the adequacy of seismic separation distances prescribed by ECP 201 by benchmarking them against detailed nonlinear time history analysis (NLTHA). Three reinforced concrete moment-resisting frame buildings—5, 8, and 11 stories—were modeled in CSI ETABS using realistic material nonlinearities, geometric nonlinearity, and bidirectional seismic excitation. Three horizontal ground motion records were selected and amplitude-scaled to ensure spectral compatibility. The NLTHA results revealed that the required separation distances were consistently larger than those calculated using ECP 201, by approximately 20% to over 100% in some configurations. The findings indicate that actual seismic demand is strongly influenced by dynamic interaction and characteristics of the applied ground motions. The results indicate that the simplified code expressions may benefit from supplementary evaluation procedures, particularly for mid-rise RC buildings in dense urban environments.

1. Introduction

In seismic regions, one of the most recurrent and critical damage mechanisms observed in urban settings is structural pounding between adjacent buildings. Pounding occurs when two structures, typically with different dynamic characteristics, vibrate out of phase during an earthquake and collide, potentially resulting in severe structural and non-structural damage, and even collapse. Historical earthquake events such as the 1985 Mexico City, 1994 Northridge, and 1999 Kocaeli earthquakes have vividly illustrated the destructive consequences of insufficient seismic separation distance [1], [2], [3]. These events triggered growing concern among structural engineers and code developers over the adequacy of existing seismic provisions, especially in densely populated urban zones where land scarcity leads to narrow building separations.

Conventional design codes, including Eurocode 8 [4], ASCE 7-22 [5], and ECP 201 [6], prescribe separation distances based on peak displacement estimates using simplified methods like the Absolute Sum (ABS) and the Square Root of the Sum of the Squares (SRSS) of peak displacements. These methods, while simple, often yield conservative or non-conservative results depending on the stiffness, mass, and dynamic properties of neighboring structures [7], [8]. Studies have demonstrated significant discrepancies between the code-prescribed separation distance and the actual displacement demands obtained via nonlinear dynamic analyses [9], [10].

To address this inadequacy, recent studies have explored advanced methods for predicting separation distances. Kamal and Inel [11] proposed simplified empirical equations derived from extensive nonlinear time history analyses (NLTHA) of RC buildings across different soil types, showing that the required seismic separation distance can be significantly larger than what codes recommend. Similarly, Flenga and Favvata [12] presented a probabilistic framework that accounts for acceptable structural pounding risk through dual-decision models, allowing either the optimization of separation distances for predefined risk levels or the assessment of acceptable risk for given separations. These probabilistic methods consider engineering demand parameters (EDPs) such as inter-story drift or relative top displacement, thereby providing more robust seismic performance assessments.

Pounding effects are not only sensitive to the relative dynamic properties of buildings, but also to their spatial configuration and construction details. Studies have shown that floor-to-column pounding results in more severe local damage compared to floor-to-floor collisions, often causing brittle failure in columns of taller structures [13]. While dampers and isolators have been proposed to mitigate pounding, these are often impractical for existing buildings. As such, accurate prediction of the required seismic separation remains the most feasible and widely applicable mitigation strategy [14].

In response to these challenges, several improved code-based and empirical approaches have been developed. Kamal [15] proposed new height-based formulas for determining separation distance without requiring full displacement analyses, making them suitable for rapid assessment of existing buildings.

Although numerous studies have investigated seismic pounding and separation distance estimation, the adequacy of the Egyptian code-prescribed separation distance has rarely been evaluated through direct comparison with bidirectional nonlinear time history analysis. This gap motivates the present study, which benchmarks the ECP 201 separation distance requirements against nonlinear dynamic displacement demands.

This study aims to evaluate the adequacy of seismic separation distances recommended by the ECP 201 through nonlinear time history analyses performed on representative building models. A series of mid-rise RC buildings (5, 8, and 11 stories) were modeled using the structural analysis software CSI ETABS [16] and subjected to bidirectional earthquake ground motions. Relative displacements are computed and benchmarked against the ECP 201 recommendations. The objective is to quantify the potential underestimation in the code and provide recommendations for revising the seismic separation distance formulas, especially for mid-rise urban buildings commonly found in Egypt.[6]

2. Numerical Modelling and Analysis Framework

2.1 Building Description

In this study, three reinforced concrete (RC) buildings were considered as representative models to investigate the adequacy of the seismic separation distance provisions defined in the Egyptian Code for Loads ECP 201. The selected buildings have five, eight, and eleven stories, respectively, and were designed to represent typical mid-rise structures commonly found in Egyptian urban contexts. The plan dimensions and story height were selected to reflect common residential building practices in Egypt. All buildings share identical plan geometry and layout, differing only in vertical configuration.

Geometrically, all buildings have a rectangular plan with overall dimensions of 30.0 meters in the longitudinal (X) direction and 24.0 meters in the transverse (Y) direction. The floor plan consists of a regular grid with five bays spaced at 6.0 meters in the X direction and four bays also spaced at 6.0 meters in the Y direction. The story height is uniform across all buildings and set to 3.0 meters per floor. All models are regular in plan and elevation, with no vertical or horizontal irregularities in geometry or mass distribution. A rectangular plan configuration was intentionally adopted instead of a square plan to achieve different lateral stiffness in the two principal directions. This modeling choice allows the buildings to exhibit different dynamic characteristics in the X and Y directions, which allows the seismic separation distance to be evaluated independently in each direction.

The structural system adopted in all three models is a special reinforced concrete moment-resisting frame (RC-MRF), wherein the lateral load-resisting system is provided exclusively through the beam–column action without the use of shear walls or bracing. This configuration was chosen to isolate the frame response and focus on the interaction between adjacent moment frames under seismic excitation. The regularity in geometry ensures that differences in seismic demand between buildings are attributed primarily to height variation rather than structural asymmetries. A schematic plan showing the bay configuration and column grid layout is presented in Figure 1, while the dimensional and reinforcement details for the vertical elements are summarized in Table 1.

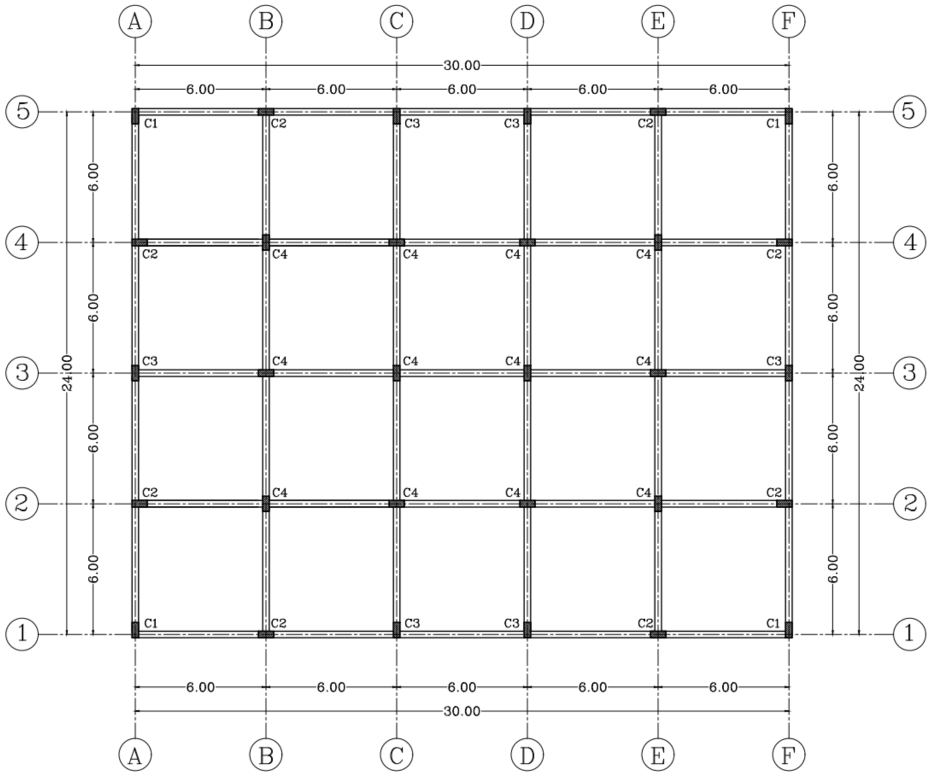

Figure 1 Typical floor plan layout

2.2 Material Properties and Section Details

All structural elements in the three modeled buildings were designed in accordance with the Egyptian Code for the Design and Construction of Reinforced Concrete Structures ECP 203 [17]. The selection of concrete and reinforcement grades reflects typical construction practices for mid-rise RC buildings in Egypt. The characteristic compressive strength of concrete was taken as $f_{cu} = 30$ MPa, and the corresponding modulus of elasticity was determined using the empirical relation recommended in ECP 203: $E_c = 4400\sqrt{f_{cu}} = 24{,}100$ MPa. The modulus of rupture in tension was estimated as: $f_{ctr} = 0.6\sqrt{f_{cu}} = 3.3$ MPa. A Poisson's ratio of 0.2 was assumed for all concrete elements.

To accurately simulate material nonlinear behavior, the stress–strain curve for confined and unconfined concrete was modeled using the Mander model, which accounts for confinement effects and nonlinear softening under high strains. For reinforcing steel, the Park model was adopted, capturing both yielding and strain hardening effects, thus enabling realistic simulation of cyclic behavior under seismic loading. Reinforcing steel was defined with a yield strength of $f_y = 420$ MPa for longitudinal reinforcement and $f_{y,\text{ties}} = 240$ MPa for column transverse reinforcement, in accordance with Egyptian standards.

The floor system in all buildings was modeled as a two-way solid slab with a uniform thickness of 160 mm, supported by beams and columns. All beams have a constant cross-section of 250 × 600 mm, while the columns vary in cross-sectional dimensions and reinforcement details depending on the gravity and seismic demand. Column design followed standard capacity-based and ductile detailing principles to ensure sufficient inelastic deformation capacity under seismic excitation. A summary of all column section dimensions and reinforcement is provided in Table 1. To account for post-cracking behavior, reduced effective stiffness modifiers were applied to all structural elements in accordance with ECP 201 [6] recommendations:

- Columns: 0.70 EI
- Beams: 0.50 EI
- Slabs: 0.25 EI

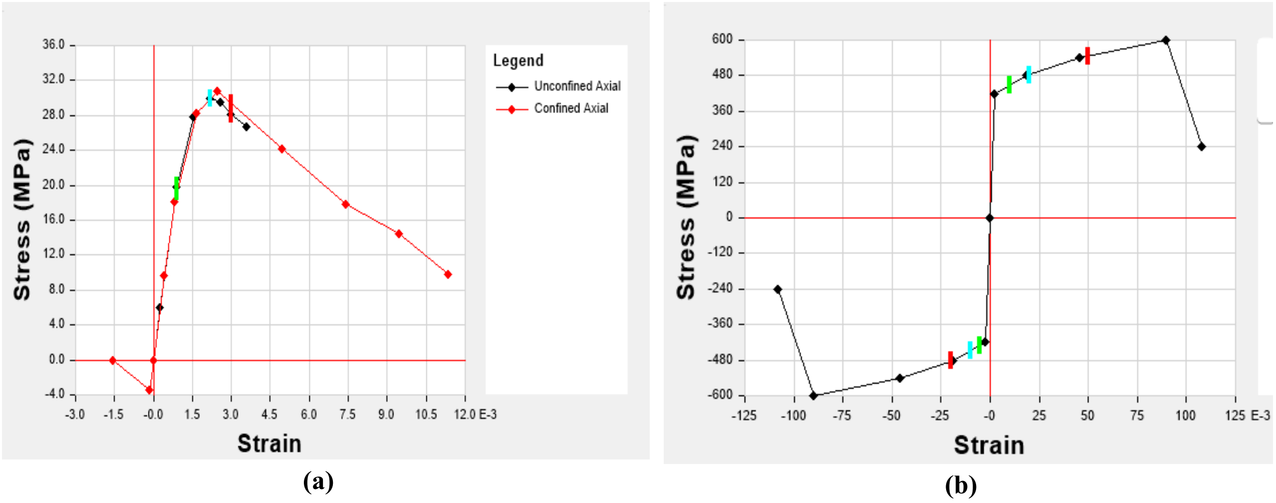

*Figure 2 Stress-strain curves for concrete and reinforcing steel. **(a)** Mander model for confined and unconfined concrete (300x900 mm column), **(b)** Park model for longitudinal reinforcement.*

Table 1 Column cross-section dimensions and longitudinal reinforcement (all dimensions in mm)

5-Story Building			8-Story Building			11-Story Building		
Type	Dimensions	Rinforcement	Type	Dimensions	Rinforcement	Type	Dimensions	Rinforcement
C1-C3	300 × 450	8T16	C1	300 × 500	8T16	C1	300 × 700	12T16
C2	350 × 650	12T16	C2-C3	300 × 600	12T16	C2-C3	300 × 900	14T16
C4	350 × 650	12T16	C4	400 × 900	18T16	C4	400 ×1300	26T16

2.3 Applied Loads

All loads were defined in accordance with the Egyptian Code for Loads and Forces ECP 201 [6] throughout the design process of structural elements. The loading types considered include gravity loads, live loads, wind loads, and seismic actions, with values selected to represent standard mid-rise construction practice in Egypt.

Dead loads consisted of the self-weight of structural elements, automatically calculated by CSI ETABS, in addition to a superimposed dead load of 1.5 kN/m² to represent floor finishes and architectural layers. Wall loads from typical masonry infill were applied as uniform line loads of 4.5 kN/m along all beams. The live load was taken as 2.0 kN/m², suitable for residential occupancy. Wind loads were applied in both orthogonal directions, based on a basic wind speed of 33 m/s. While wind was considered in the code-based design combinations, it was not the focus of the time history analysis in this study.

Regarding seismic loading, the buildings were assumed to be located in seismic Zone 3, resting on a class C soil profile, as defined by ECP 201 [6]. A Type 1 response spectrum was adopted, consistent with the expected seismicity level of the region. The importance factor was taken as $\gamma_I = 1.0$, and the response modification factor as $R = 5.0$, corresponding to special reinforced concrete moment-resisting frame systems. A structural damping ratio of 5% was used in both the design and nonlinear time history analyses. The seismic mass source in CSI ETABS was defined using the full dead load plus 25% of the live load, in accordance with ECP 201 [6] provisions. This mass definition was consistently used in both modal and time history analyses to ensure accurate dynamic response evaluation.

3. Nonlinear Dynamic Analysis Framework

3.1 Selection of Ground Motions

The selection of ground motion records is a critical step in nonlinear time history analysis (NLTHA), particularly when the objective is to evaluate sensitive response parameters such as relative displacements between adjacent buildings.

Unlike linear response spectrum analysis, which uses idealized code-based spectra, NLTHA relies on real-time acceleration records to simulate the actual time-dependent response of structures. However, not all earthquake records are directly usable in their raw form. Proper selection must ensure that the chosen ground motion records are representative of the seismic hazard scenario and site conditions, and that they are compatible with the characteristics of the structural system being analyzed.

According to ECP 201 [6], when NLTHA is used for seismic design or evaluation, a minimum of three ground motion records must be used. When only three records are used, the maximum response values from each analysis are to be taken without averaging. This approach ensures that the analysis remains conservative and captures a reasonable upper-bound estimate of structural demand. Similar provisions exist in international codes such as ASCE 7-22 [5], and Eurocode 8 [4]. In this study, ground motions were selected from the PEER Ground Motion Database [18] to reflect the assumed site conditions, the records were filtered based on several key parameters: (Mw) range of 5.0 to 7.0, a shear wave velocity (V_{s30}) range of 180–360 m/s consistent with Soil Type C, a minimum PGA of 0.10 g to ensure sufficient intensity, and an initial scale factor range of 0.7 to 1.5 to maintain realism during amplitude adjustment. These bounds ensured that the selected ground motions were compatible with the seismic hazard profile.

Each ground motion was obtained in the form of three separate acceleration records, corresponding to two orthogonal horizontal components and one vertical component. These files were individually downloaded from the PEER Ground Motion Database. In this study, only the horizontal components (H1 and H2) were utilized, as the objective was to assess lateral relative displacements between adjacent buildings, which are the primary cause of seismic pounding. The vertical component was intentionally excluded, consistent with common practice in pounding-focused evaluations involving regular RC moment-resisting frame systems without significant vertical discontinuities. The scaling methodology applied to these selected ground motions is detailed in the following subsection.

3.2 Scaling of Ground Motions

Ground motion records collected from real earthquakes often exhibit significant variation in amplitude and spectral content when compared to idealized code-based design spectra. This disparity can lead to misleading conclusions in nonlinear dynamic analysis (NLTHA) if ground motion records are used without proper scaling. To ensure spectral compatibility with the target design spectrum defined by ECP 201[6] for Seismic Zone 3 and Soil Class C, each selected ground motion was scaled appropriately. This scaling process is essential to avoid over- or under-representation of certain spectral periods, particularly those near the fundamental modes of the studied buildings.

Two principal approaches are commonly used to adjust ground motion intensity for structural analysis: spectral matching and amplitude scaling. Spectral matching modifies the frequency content of the motion to artificially align with the target response spectrum. While effective in shape fitting, it can distort the original energy distribution and temporal characteristics of the signal. In contrast, amplitude scaling applies a uniform scale factor to the entire record, thereby preserving the natural frequency content, impulsiveness, and energy concentration of the original motion. For this reason, amplitude scaling was adopted in the present study.

Although ECP 201 does not prescribe a detailed procedure for ground motion scaling, the methodology was aligned with international best practices, specifically according to Section 16.2.3.2 of ASCE 7-22 [5], scaling should be performed using the RotD100 response spectrum, which represents the maximum-direction spectral acceleration obtained by rotating the two horizontal components (H1 and H2) through all possible angles (0° to 180°). This approach replaces the older SRSS (Square Root of Sum of Squares) method, providing a more conservative and physically meaningful measure of structural demand, especially for irregular or asymmetric buildings. In this study, RotD100 spectra were computed using the online scaling tool provided by the PEER Ground Motion Database, which automatically calculates the rotation-based spectral envelope across a user-defined period range. The target spectrum was defined in accordance with ECP 201, based on Seismic Zone 3, Soil Type C, and Importance Factor $\gamma_I = 1.0$.

A single amplitude scale factor was applied to both H1 and H2 components of each record, as required by ASCE 7-22 and implemented in most NLTHA frameworks. After computing the RotD100 spectrum for each record and comparing it to the target design spectrum, appropriate scale factors were derived. The selected ground motions, along with their final scale factors and key metadata, are summarized in Table 2.

Table 2 Characteristics of selected ground motions

RSN	Earthquake Name	Year	Scale Factor	Magnitude (Mw)	Vs30 (m/s)
309	SMART1 (Taiwan)	1981	1.1993	5.9	268
530	N. Palm Springs (USA)	1986	0.9309	6.06	312
5263	Chuetsu-oki (Japan)	2007	0.7164	6.8	274

To visually demonstrate the effectiveness of the scaling process, two comparative spectral plots are provided. Figure 3 presents the original response spectra of the selected records prior to scaling, plotted alongside the target ECP design spectrum. Figure 4 shows the RotD100 spectra of the scaled horizontal components, revealing a close match with the code-defined spectral shape. This alignment confirms the validity of the adopted amplitude scaling methodology and its suitability for nonlinear time history analysis of the selected models.

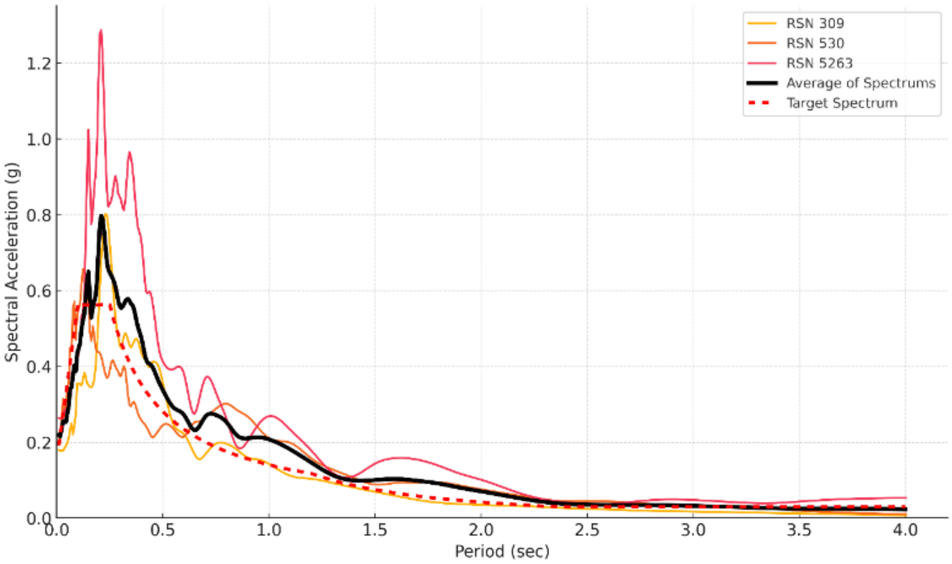

Figure 3 The spectrum of unscaled records

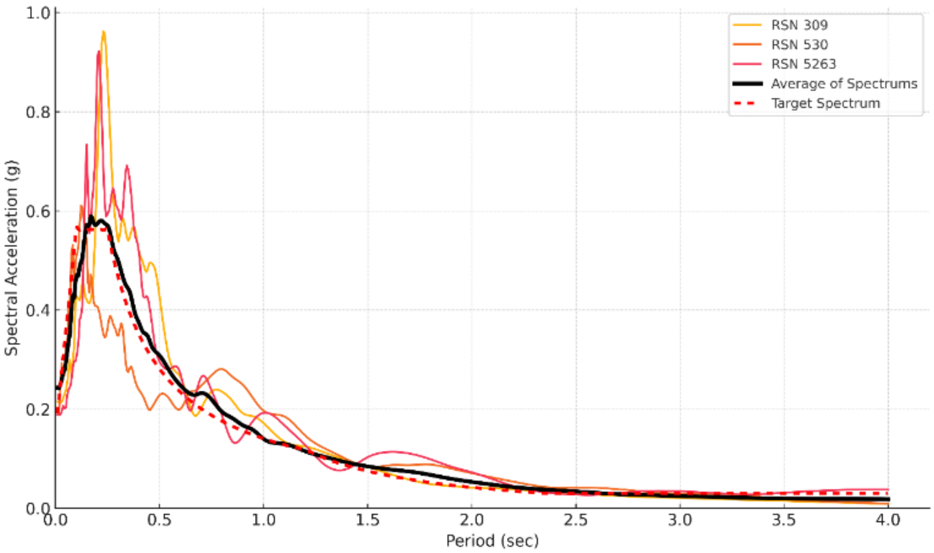

Figure 4 The RotD100 spectrum of scaled records

3.3 Time History Analysis Configuration

To accurately assess the potential for seismic pounding between adjacent buildings, the current study employed nonlinear time history analysis (NLTHA), which is widely regarded as the most realistic and informative method for capturing seismic response under real ground motion scenarios. Unlike response spectrum analysis, which simplifies the excitation into an envelope of maximum responses, NLTHA preserves time-dependent dynamic interactions, phase differences, and impulsive characteristics of real earthquakes, all of which are critical for modeling inter-building collisions.

The analysis was conducted using CSI ETABS, and the NLTHA was configured as a nonlinear direct integration time history method, explicitly solving the equations of motion without modal decomposition. Time integration was carried out using the Hilber-Hughes-Taylor (HHT) method, a robust implicit algorithm widely adopted in nonlinear structural dynamics. A value of $\alpha = -1/24$ was used, providing critical damping in high-frequency modes while preserving accuracy in the low-frequency response. Compared to the more conventional Newmark method, the HHT formulation offers superior numerical stability, especially in nonlinear or stiff systems. A structural damping ratio of 5% was assumed for all modes, consistent with reinforced concrete construction and the design-level intensity of the ground motions.

Each ground motion record was applied using its two perpendicular horizontal components (H1 and H2), downloaded from the PEER Ground Motion Database. To capture bidirectional excitation effects, two distinct load cases were created for each record, as illustrated in Figure 5:

- Load Case 1: H1 applied in the X-direction, H2 in the Y-direction.
- Load Case 2: H2 applied in the X-direction, H1 in the Y-direction.

This approach ensures that each structure is subjected to the full variability of directional excitation, capturing critical relative displacement patterns in both principal axes. In total, three ground motion records were used, resulting in six nonlinear time history load cases. For each earthquake record, the required separation distance was computed independently for each load case, and the larger of the two values was adopted as the representative safe distance for that record.

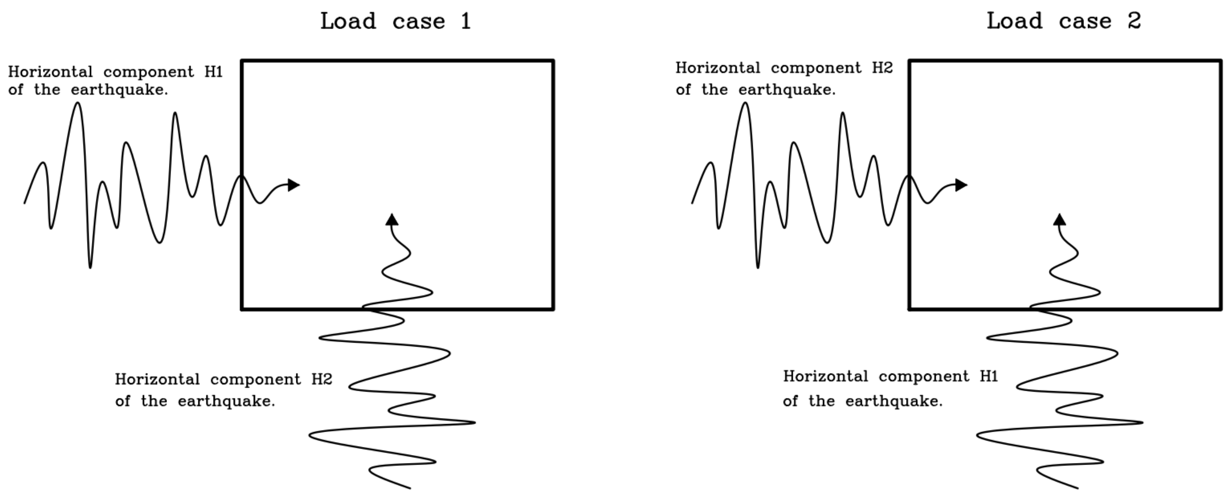

Figure 5 Bidirectional application of ground motion components

3.4 Nonlinear Modeling Assumptions

To realistically simulate the structural behavior of reinforced concrete frames under seismic excitation, the analysis incorporated both material and geometric nonlinearities, along with explicitly defined localized inelasticity at the member level. These modeling decisions allow the analysis to capture critical response characteristics such as energy dissipation, strength degradation, and redistribution of internal forces.

Material nonlinearity was introduced using established constitutive models. Concrete behavior was modeled using the Mander stress-strain relationship, which accounts for confinement effects and post-peak softening, particularly in regions confined by transverse reinforcement. Reinforcing steel was defined using the Park model, which provides a bilinear elasto-plastic response with strain hardening, allowing for accurate simulation of yielding and cyclic behavior in longitudinal reinforcement.

Geometric nonlinearity was activated using the P–Δ plus large displacement formulation available in CSI ETABS. This configuration accounts for both classical P–Δ effects due to axial forces acting through lateral displacements, and higher-order geometric stiffness changes under large deformations. While the influence of geometric nonlinearity is typically moderate in mid-rise structures, its inclusion enhances consistency in the nonlinear framework and enables proper capture of displacement-dependent force redistribution that may affect inter-building response.

Nonlinearity at the member level was explicitly modeled using both plastic hinges and fiber hinges, depending on the element type and behavioral role. Beams were assigned predefined plastic hinges at both ends, following the guidelines of ASCE 41-17 [19], Table 10-7 (Concrete Beams – Flexure, Item i), which standardizes moment–rotation behavior under cyclic loading. For columns, nonlinear behavior was represented using fiber-type P–M2–M3 hinges defined at both ends, with a hinge length of 350 mm. The fiber hinge approach enables detailed simulation of axial–bending interaction using layered cross-sectional behavior under inelastic demand. Through this combination of material, geometric, and localized nonlinear modeling, the analytical framework achieves a realistic and code-compliant representation of RC frame behavior, enabling reliable estimation of inter-story drift and separation distance demands under dynamic excitation.

4. Seismic Separation Distance: Code-Based and Analytical Evaluation

4.1 Code-Based Estimation of Separation Distance

The Egyptian Code for Loads ECP 201 [6] requires a minimum separation distance between adjacent buildings to prevent structural pounding during seismic events. The code accounts for the possibility of out-of-phase lateral movement between neighboring structures and prescribes a method to compute the required separation distance accordingly. For adjacent buildings without aligned floor levels, the required separation distance is calculated as the square root of the sum of the squares of the expected lateral displacements of the two buildings at the same elevation, typically the height of the shorter building:

$$S_{\mathrm{min}} = \sqrt{(\Delta_1)^2 + (\Delta_2)^2} \tag{1}$$

where:

Δ_1, Δ_2: lateral displacements of each building at the potential pounding level.

However, if the buildings have identical floor levels, Clause 8-8-2-7-2 of ECP 201 [6] permits a 70% reduction in the required separation distance, leading to the following simplified expression:

$$S_{\mathrm{reduced}} = 0.3 \times \sqrt{(\Delta_1)^2 + (\Delta_2)^2} \tag{2}$$

It is important to emphasize that the lateral displacements Δ_1 and Δ_2 used in the code-based separation distance formula are not taken directly from the raw results of RSA. Instead, they are calculated in accordance with this code-defined expression.

$$d_s = 0.7\, R\, d_e \tag{3}$$

where:

d_s: displacement used in the separation distance formula

R: response modification factor

d_e: displacement obtained from linear analysis

In order to apply the code-based separation formulas described earlier, it was essential to first determine the expected lateral displacements of each building under seismic loading. To achieve this, all three structures - the 5-story, 8-story, and 11-story buildings - were subjected to response spectrum analysis (RSA) in both the X and Y directions. This analysis provided an estimate of the peak dynamic response at each floor. Displacements were extracted at every floor level; however, for the purpose of assessing the risk of seismic pounding, only specific levels are relevant - namely, those where adjacent buildings have aligned floor elevations and where impact is most likely to occur. These typically include the top floor of the shorter building in each pair. As a result, the reported displacement values focus on these pounding-relevant floors only. Figure 5 illustrates the maximum lateral displacements obtained from RSA at these critical levels, shown for both the X and Y directions. These values represent the basis for computing the code-prescribed separation distance between buildings. The final separation distances calculated using the code-based approach from RSA results are illustrated in Figure 6. As shown, the values vary between configurations, with the B8‖B11 pair in the Y-direction exhibiting the largest requirement. These results serve as a reference baseline against which the time-history-based separation distance estimations can be compared.

4.2 Nonlinear Time History-Based Evaluation of Separation Distance

To evaluate the required seismic separation distance between adjacent buildings, the relative displacement response of each model was analyzed using the nonlinear time history results obtained under three different ground motions. For each simulation, displacement data were extracted at every time step for all relevant floor levels. In each building pair, the pounding risk was evaluated at the same elevation in both structures, typically the top floor of the shorter building, where the largest relative displacement and potential impact were most likely to occur.

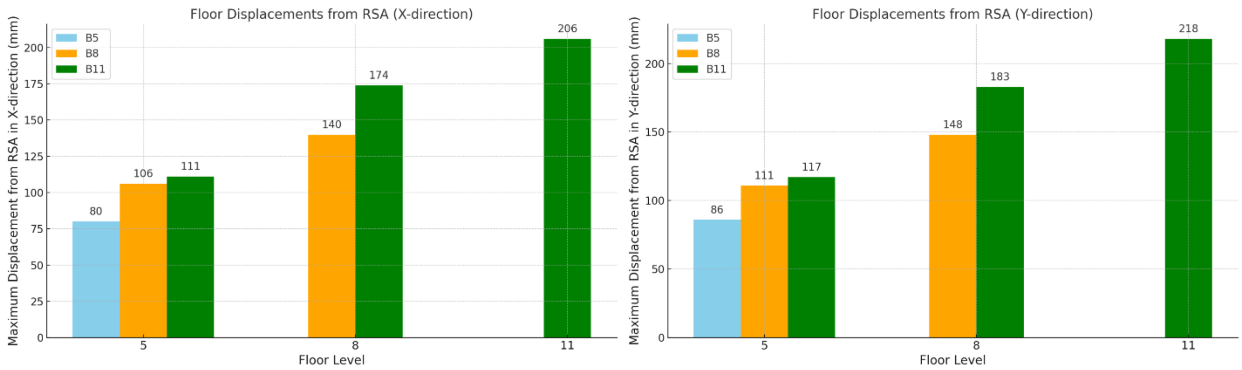

Figure 6 RSA-based lateral displacements at critical floors in X and Y directions.

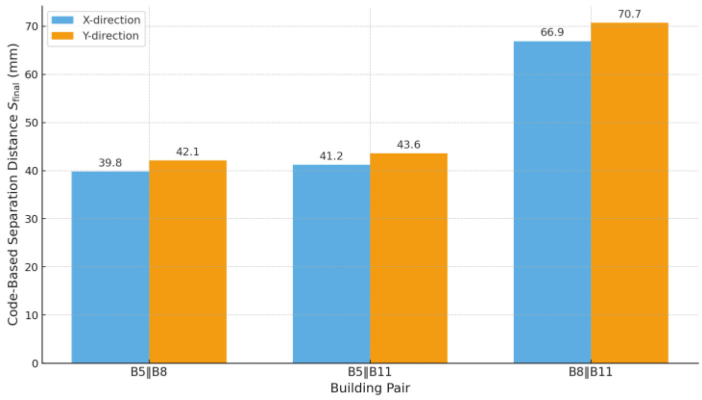

Figure 7 Final required separation distance from code-based calculations

To assess the possibility of collision at any point during the seismic response, the following expression was used to compute the relative displacement between the two buildings at each time step:

$$s(t) = u_1(t) - u_2(t) \tag{4}$$

where:

$u_1(t)$: Lateral displacement of the first building at time t,

$u_2(t)$: Lateral displacement of the adjacent building at the same floor level and at the same instant t,

$s(t)$: Instantaneous relative distance between the two structures.

This relation was evaluated at every time step throughout the earthquake duration. If $s(t) < 0$, no contact occurs at that instant, and the buildings remain separated. However, if $s(t) > 0$, it indicates that pounding would occur unless a physical separation of at least $s(t)$ exists between the buildings at that specific moment. Therefore, the maximum positive value of $s(t)$ was taken as the minimum required separation distance for that building pair under the given ground motion:

$$S_{\min} = \max_t\big(u_1(t) - u_2(t)\big) \quad \text{for } s(t) > 0 \tag{5}$$

This procedure was repeated for all three ground motion records. For each building pair, three distinct values of $S_{\min}$ were obtained. In accordance with the provisions of ECP 201 [6], the largest of these values was adopted as the required separation distance:

$$S_{\text{final}} = \max(S_1, S_2, S_3) \quad (6)$$

Where each S_i corresponds to the result from one building pair.

This method was systematically applied to all studied combinations of building heights and adjacency directions. For each pair of buildings, two distinct spatial configurations were considered based on their relative placement within the plan: In the X-direction configuration, the two buildings were placed side by side along their 30 m facades, such that the separation distance and expected pounding occurred along the global X-axis. In the Y-direction configuration, the same buildings were placed adjacent along their 24 m facades, such that the potential pounding occurred along the global Y axis. These two configurations are denoted respectively as: $B_i \parallel B_j$. All combinations of building pairs—namely, $B_5 \parallel B_8$, $B_5 \parallel B_{11}$, and $B_8 \parallel B_{11}$ —were analyzed in both directions.

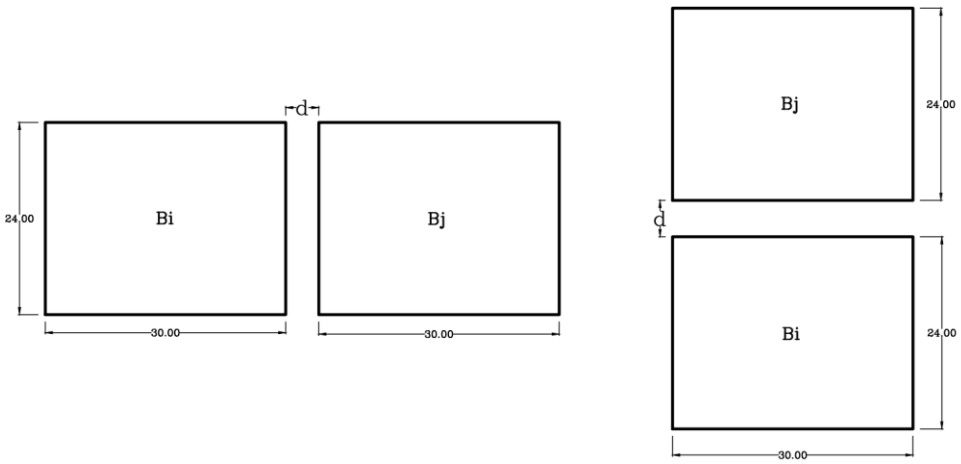

Figure 8 Two spatial configurations of adjacent buildings: X-direction and Y-direction

Prior to conducting the parametric study on adjacent building configurations, the numerical models were evaluated to ensure that their global dynamic response, displacement profiles, and fundamental vibration characteristics were consistent with expected structural behavior for mid-rise reinforced concrete moment-resisting frames.

The outcomes of the NLTHA procedure described previously are presented in Table 3 and visualized in figure 9. To better visualize the seismic interaction that leads to the critical separation demand, figure 8 shows the time history of relative displacement between the B8 and B11 buildings when placed adjacent in the Y-direction. This configuration was found to produce the largest required separation distance among all studied cases. Each plot corresponds to a different ground motion record and captures the relative movement $s(t) = u_8(t) - u_{11}(t)$ over time at the same floor level, illustrating the dynamic nature of potential pounding.

Table 3 Separation distances (mm) for each building pair.

Building Pair	Configuration	RSN309	RSN530	RSN5263	S_{final}
B5 ‖ B8	X	48.2	70.0	81.3	81.3
B5 ‖ B8	Y	48.5	72.6	78.4	78.4
B5 ‖ B11	X	58.2	62.8	66.5	66.5
B5 ‖ B11	Y	56.2	60.2	62.3	62.3
B8 ‖ B11	X	63.7	81.5	77.1	81.5
B8 ‖ B11	Y	65.3	83.8	76.7	83.8

As shown, the required separation distance varies significantly depending on both the combination of buildings and the direction in which they are placed adjacent to one another. These trends are clearly reflected in the chart, which enables direct comparison across configurations. The B8‖B11 pair in the Y-direction exhibited the largest separation requirement overall, with a final separation distance of 83.8 mm. Together, the tabulated and graphical results capture the full range of dynamic interaction between adjacent structures and emphasize the importance of direction-specific evaluation when determining seismic separation requirements. These findings offer a more realistic and case-specific foundation for safe seismic design compared to simplified code-based estimates.

4.3 Comparison Between Code-Based and NLTHA-Derived Separation Distances

This subsection presents a direct comparison between the minimum separation distances prescribed by code provisions and those obtained from nonlinear time history analysis (NLTHA). For each building pair and configuration, the final code-based separation distance was computed in accordance with ECP 201, while the corresponding NLTHA values reflect the actual maximum relative displacements observed under dynamic excitation. The two sets of values are plotted side-by-side in figure 10.

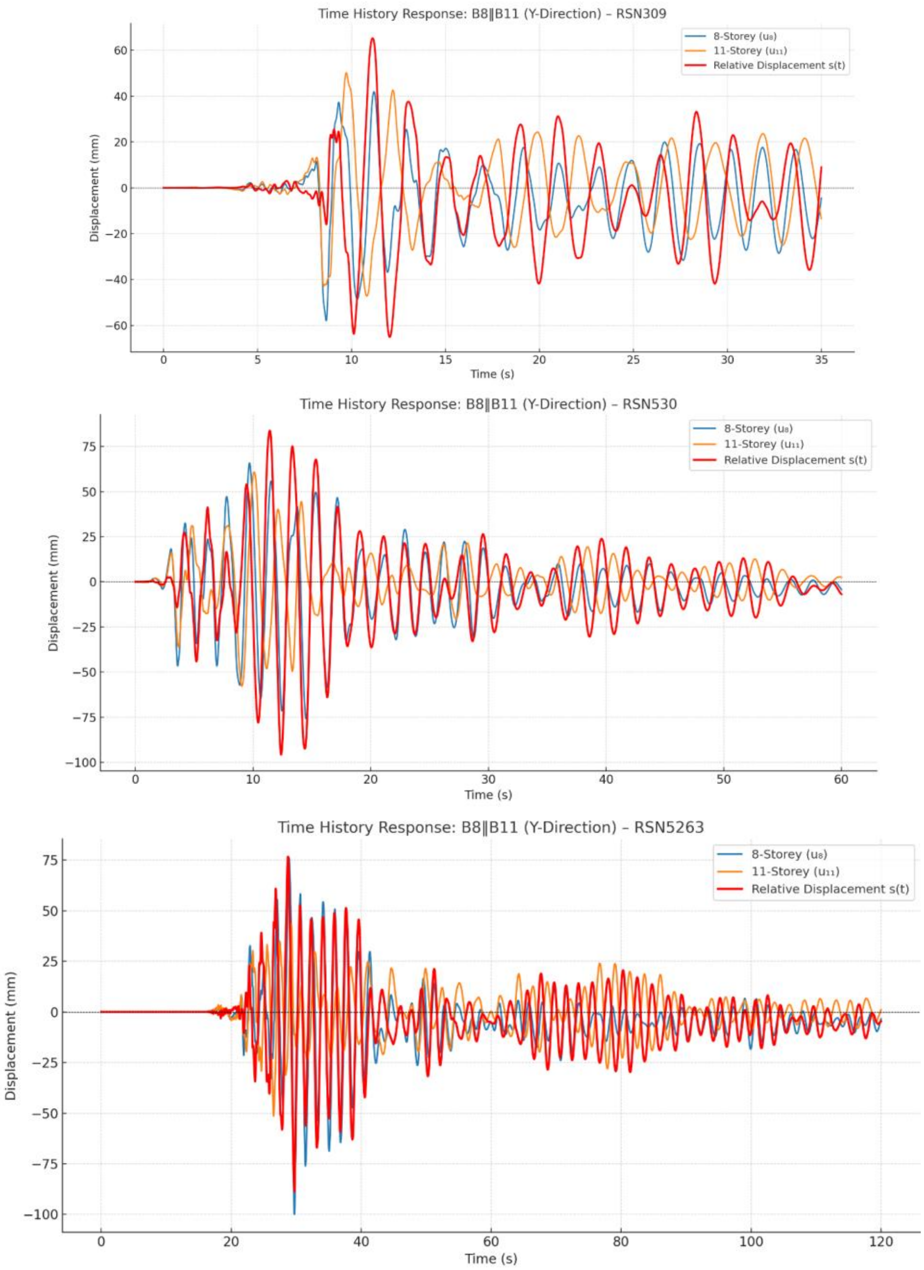

Figure 9 Relative displacement time history for B8‖B11 in Y-direction

Across all studied cases, the NLTHA-derived distances were consistently higher than those recommended by the code. To evaluate the magnitude of this discrepancy, a normalized ratio was calculated as ratio $= S_{\text{NLTHA}}/S_{\text{code}}$, and the results are shown in figure 11. A ratio greater than 1.0 indicates that the code-prescribed separation is insufficient to prevent collision under realistic seismic motion. The most critical case was observed in the B5‖B8 pairing along the X-direction, where the required separation distance from NLTHA was more than twice the value suggested by the code.

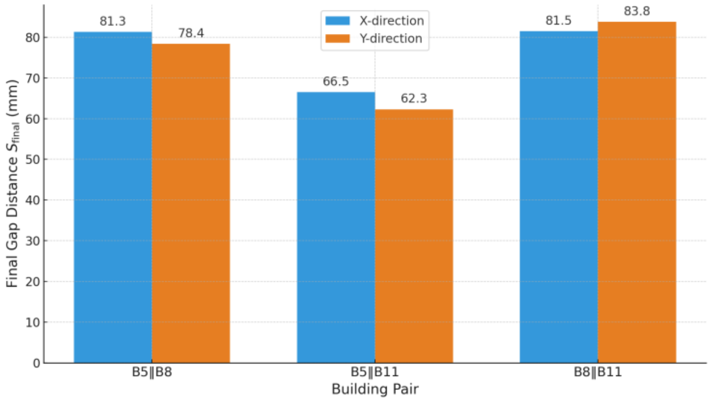

Figure 10 Final separation distance from NLTHA results

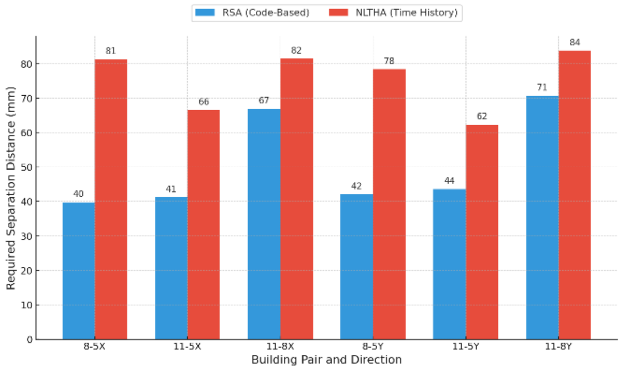

Figure 11 Comparison of code-based and NLTHA separation distances

These findings highlight a potential vulnerability in relying exclusively on simplified code formulations when designing adjacent buildings. While code equations offer practical approximations for general use, they may fail to capture the full extent of transient relative motion during seismic events. For densely packed urban environments or configurations involving significant structural disparity, incorporating NLTHA in the design phase can lead to more robust and reliable separation distance recommendations, ensuring that seismic pounding is effectively avoided.

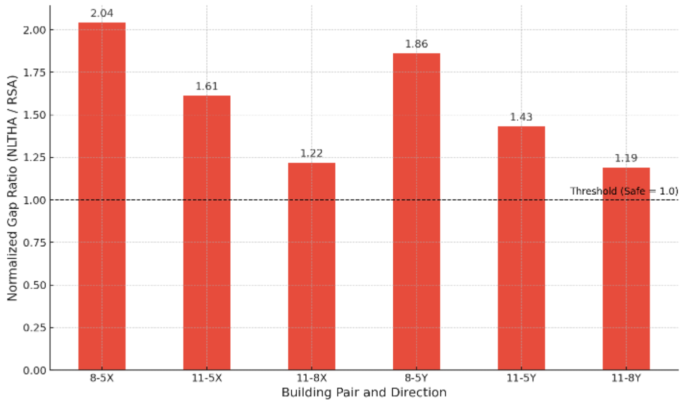

Figure 12 Normalized NLTHA-to-code separation distance ratios

5. Conclusions

In summary, the results demonstrate that the seismic separation distances prescribed by ECP 201 may underestimate the actual displacement demands for mid-rise reinforced concrete buildings subjected to bidirectional ground motions. The nonlinear time history analyses highlight the influence of building height and directional stiffness on the required separation distance. These findings emphasize the need for revisiting the simplified separation formulas adopted in the Egyptian code to ensure adequate seismic performance in dense urban environments.

The main findings of the present study can be summarized as follows:

- In all building configurations, the separation distances obtained from nonlinear time history analysis (NLTHA) exceeded those prescribed by the ECP 201 code, indicating that the code expressions may lead to unconservative designs when applied to adjacent mid-rise RC buildings of different heights.
- The difference between code-based and NLTHA-derived separation distance values reached up to 104% in some cases.
- The required separation distance was found to be affected by the combination of building heights and their dynamic interaction.
- The consistent exceedance of NLTHA-based separation distance over code values indicates that, in certain configurations, the implicit safety margin associated with code-based separation distances may be smaller than intended when adjacent mid-rise buildings are considered.
- While code-based formulas provide a practical first estimate, the results suggest that detailed nonlinear analysis can offer more accurate and safer design recommendations for critical configurations, particularly in dense urban settings.
- These findings may support the refinement of current code provisions by introducing optional correction factors or adjustment coefficients for mid-rise adjacent buildings, especially when adjacent buildings have different dynamic properties.

6. References

[1] R. Jankowski, "Non-linear FEM analysis of earthquake-induced pounding between the main building and the stairway tower of the Olive View Hospital," *Eng. Struct.*, vol. 31, no. 8, pp. 1851–1864, 2009.

[2] P. C. Polycarpou and P. Komodromos, "Numerical investigation of potential mitigation measures for poundings of seismically isolated buildings," *Earthq. Struct.*, vol. 2, no. 1, pp. 1–24, 2011.

[3] S. A. Anagnostopoulos, "Pounding of buildings in series during earthquakes," *Earthq. Eng. Struct. Dyn.*, vol. 16, no. 3, pp. 443–456, 1988.

[4] European Committee for Standardization (CEN), "Eurocode 8: Design of Structures for Earthquake Resistance – Part 1: General Rules, Seismic Actions and Rules for Buildings," Brussels, Belgium, 2004.

[5] American Society of Civil Engineers (ASCE), "Minimum Design Loads and Associated Criteria for Buildings and Other Structures (ASCE/SEI 7-22)," Reston, VA, USA, 2022.

[6] Housing and Building National Research Center (HBRC), "Egyptian Code for Calculation of Loads and Forces in Structural and Building Works (ECP 201)," Cairo, Egypt, 2012.

[7] M. Kamal and M. Inel, "Simplified approaches for estimation of required seismic separation distance between adjacent reinforced concrete buildings," *Eng. Struct.*, vol. 252, p. 113610, 2022.

[8] Y. Jaradat, H. Far, and M. Mortazavi, "A Mathematical Approach for Predicting Sufficient Separation Gap between Adjacent Buildings to Avoid Earthquake-Induced Pounding," *Civ. Eng. J.*, vol. 9, no. 10, pp. 2370–2398, 2023.

[9] M. Kamal, M. Inel, and B. T. Cayci, "Seismic behavior of mid-rise reinforced concrete adjacent buildings considering soil-structure interaction," *J. Build. Eng.*, vol. 51, p. 104296, 2022.

[10] G. D. Awchat, A. Monde, R. Sirsikar, R. Dingane, and G. Dhanjode, "Seismic Pounding Response of Neighboring Structure using Various Codes with Soil-Structure Interaction effects: Focus on Separation Gap," *Civ. Eng. J.*, vol. 8, no. 2, pp. 308–318, Feb. 2022, doi: 10.28991/CEJ-2022-08-02-09.

[11] M. Kamal and M. Inel, "A new equation for prediction of seismic gap between adjacent buildings located on different soil types," *J. Build. Eng.*, vol. 57, Oct. 2022, doi: 10.1016/j.jobe.2022.104784.

[12] M. G. Flenga and M. J. Favvata, "A New Method for Defining the Optimal Separation Gap Distance and the Acceptable Structural Pounding Risk on Multistory RC Structures," *Appl. Sci.*, vol. 14, no. 3, p. 1165, 2024.

[13] S. M. Khatami *et al.*, "Effective Gap Size Index for Determination of Optimum Separation Distance Preventing Pounding between Buildings during Earthquakes," 2021, doi: 10.3390/app1105.

[14] S. E. A. Raheem, “Pounding mitigation and unseating prevention at expansion joints of isolated multi-span bridges,” *Eng. Struct.*, vol. 31, no. 10, pp. 2345–2356, 2009.
[15] M. Kamal, “Code-based new approaches for determining the minimum required separation gap,” in *Structures*, Elsevier, 2022, pp. 750–764.
[16] Computers and Structures Inc. (CSI), “ETABS: Integrated Building Design Software, Version 20,” Berkeley, CA, USA, 2020.
[17] Housing and Building National Research Center (HBRC), “Egyptian Code for Design and Construction of Reinforced Concrete Structures (ECP 203),” Cairo, Egypt, 2020.
[18] Pacific Earthquake Engineering Research Center (PEER), “PEER Ground Motion Database.” < https://peer.berkeley.edu/peer-strong-ground-motion-databases>
[19] American Society of Civil Engineers (ASCE), “Seismic Evaluation and Retrofit of Existing Buildings (ASCE/SEI 41-17),” Reston, VA, USA.